ELSEVIER

Materials Science and Engineering A 422 (2006) 3–18

MATERIALS SCIENCE & ENGINEERING A

www.elsevier.com/locate/msea

Intergranular glassy films: An overview

Anandh Subramaniam [a,*], Christoph T. Koch [b], Rowland M. Cannon [c], Manfred Rühle [b]

[a] *Indian Institute of Technology, New Delhi 110016, India*
[b] *Max-Planck-Institut für Metallforschung, Heisenbergstr. 3, 70569 Stuttgart, Germany*
[c] *Lawrence Berkeley National Laboratory, University of California, Berkeley, CA 94720, USA*

Received in revised form 24 November 2005

Abstract

In certain ceramics like Si_3N_4, SiC, $SrTiO_3$, Al_2O_3, etc., the grain boundary (GB) region can have an amorphous film of about 1–2 nm thickness. These intergranular glassy films (IGFs) are characterized by a nearly constant thickness which is basically independent of the orientation of the bounding grains, but is dependent on the composition of the ceramic. The IGF is resistant to crystallization and is thought to represent an equilibrium configuration. The presence of the IGF, along with its structure, plays an important role in determining the properties of the ceramic as a whole. Important amongst these properties, keeping in mind the system based specificities, are fracture, creep, oxidation and electrical behaviour. Depending on the system, various synthetic routes like liquid phase sintering, solid-state activated sintering, crystallization of glass surrounding the crystal, etc., have led to the formation of IGFs. Equilibrium thickness amorphous films on surfaces have also been synthesized which are considered to be the surface analogue of IGFs. Important advances in the microscopy techniques have provided invaluable insights into the structure of IGFs, along with its interface with the bounding crystals. These techniques include: high-resolution microscopy, Fresnel contrast imaging, diffuse dark field imaging, diffraction analysis, electron holography, high-angle annular dark field imaging, energy-dispersive X-ray analysis and electron energy loss spectroscopy. It is now being progressively realized that the composition and structure within the IGF is graded, i.e., it has a diffuse interface with the bounding crystals and that the amorphous material in the IGF is different from the bulk glass forming in that system. The order induced by the bounding crystals on the IGF is seen as a contributing factor to the gradation. In spite of the achievements, a lot of open questions remain regarding the formation of IGFs, its behaviour with temperature, its dependence on crystallography of the bounding grains, etc. This overview aims at introducing IGFs to a non-specialist audience, summarizing the important advances in the field and outlining the outstanding issues.

Keywords: Intergranular glassy film; Amorphous structure; Equilibrium thickness; Partial ordering; Diffuse interface; Transmission electron microscopy; Colloidal behaviour

1. Introduction

Amongst conceivable descriptions of grain and heterophase interfaces (Fig. 1), boundaries having an "equilibrium thickness intergranular glassy film" (IGF for short) (Fig. 2) form a special class on its own, characterized by a nearly constant thickness (of about 1–2 nm) for a given composition; which is basically independent of the orientation of the bounding grains.

The structure of the IGF has a profound influence on the properties of the ceramic. Important among these properties are creep resistance, oxidation resistance and fracture toughness. The IGF also plays an important role in determining the electrical properties in ceramics like ZnO and $SrTiO_3$.

The last few decades have seen tremendous progress in the experimental (Section 4) and theoretical (Section 3) front, which has led to a much better understanding of IGFs. This has been possible due to parallel advancement in microscopes and microscopy techniques (Section 2).

It is seen that IGF can arise from various synthetic routes like liquid phase sintering, solid state sub-eutectic sintering, crystallization of the glass surrounding a ceramic crystal, etc. (Section 4.1). Equilibrium amorphous films on surfaces, considered to be the surface analogue of IGF have also been synthesized (Section 4.1.6). The effect of various stimuli and treatments, like pressure, annealing, creep, etc., on the evolution of the IGF has also been a subject of interesting study (Section 4.2).

At this point it is not clear as to what the common factors are amongst IGFs forming in various systems, nor are the key differences well understood. Even from a simple thickness mea-

* Corresponding author. Tel.: +91 11 2659 1340; fax: +91 11 2658 1119.
E-mail address: anandh333@rediffmail.com (A. Subramaniam).

0921-5093/$ – see front matter © 2006 Elsevier B.V. All rights reserved.
doi:10.1016/j.msea.2006.01.004

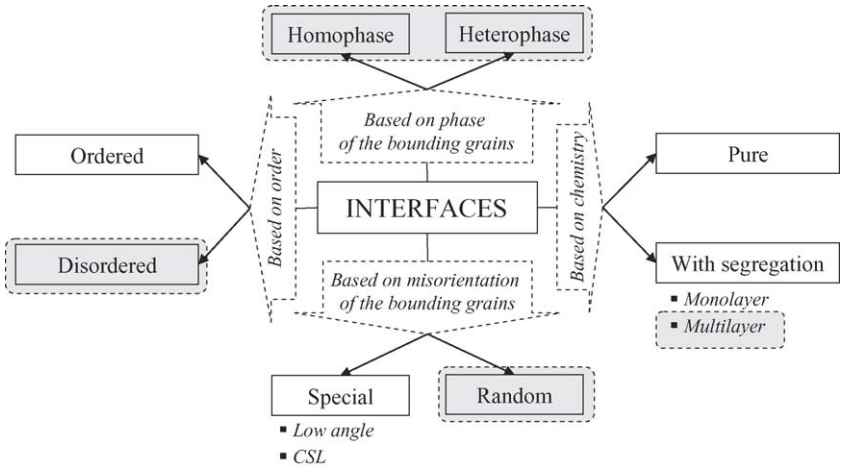

Fig. 1. Possible ways of looking at internal interfaces in materials. The descriptions that fit intergranular glassy films have been shaded.

surement perspective, straight grain boundaries (GBs) can be found in Si_3N_4, making measurements easier and reliable, while in other systems (e.g. SiC, $SrTiO_3$, etc.) the GBs with IGF are usually curved, making certain kinds of analysis more difficult.

This overview aims at introducing IGFs to a general/non-specialist audience, summarizing the important advances in the field and outlining the outstanding issues. Keeping this in view, a textbook style approach has been used with figures and bulleted points. Though IGFs are reported in many systems, much of the research work has focused on Si_3N_4, ZnO (Bi_2O_3 doped) and SiC and hence most of this overview will discuss results from these systems. Attempt has also been made to keep references to an optimum level, limiting ourselves to what we considered good starting points for searching more detailed information. References have been left out from the starting paragraphs of the introduction section and have been inserted in the appropriate sections for easy classification based on subject.

The terms IGF, amorphous film and film have been used interchangeably and as mentioned before IGF connotes equilibrium thickness. The acronym IGF has also been used for amorphous films at heterophase interfaces and refers to *equilibrium* configuration amorphous films with widths in the range of 1–2 nm. The words thickness and width are also used interchangeably. Dry boundaries refer to grain boundaries without an IGF. The phrase "complete wetting" shall imply that the thickness of the material between the grains can increase indefinitely, which automatically implies the lack of formation of an IGF. Special grain boundaries are near Sigma boundaries and random boundaries are high-angle non-special boundaries.

The terms "triple pocket", "triple point" and "pocket" are used seemingly interchangeable throughout literature and refer to junctions of more than just two grains. While triple lines are formed along the intersection of three grains sharing an edge, the term "triple point" should be avoided in this context since the junction of at least four grains is required to define a point in three dimensions. In this review we will use the term "pocket" to describe general intergranular bodies of amorphous material not falling into the category "IGF".

Some basic points about IGFs are:

- Systems in which IGFs have been observed:
  - ceramic–ceramic interface: Si_3N_4 (undoped and doped with MgO, Y_2O_3, rare-earth oxides, CaO, F, Cl) [1], SiC [2], Al_2O_3 [3], $SrTiO_3$ [4], ZnO (Bi_2O_3 doped) [5,6], Si_2N_2O [7], SiAlON [1], TiO_2–SiO_2 [8], mullite [9];
  - ceramic–ceramic heterointerface in composites: ruthenate (Ru_2O, Pb_2 Ru_2O_7, Bi_2 Ru_2O_7)–silicate glass (PbO–Al_2O_3–TiO_2–SiO_2) composites [10], Si_3N_4–SiC [11];
  - metal–ceramic interface: Al_2O_3–Cu, Al_2O_3–Ni [12], Si_3N_4–Al [13];
  - in addition to the grain boundaries IGFs are also found between the crystallized triple pocket phase and the grains in Si_3N_4 and SiC;
  - amorphous surface films also show equilibrium thickness: $Si_{1-x}Zr_xO_2$ films on Si, Bi_2O_3 films on ZnO.
- Constant thickness (~1–2 nm) *basically*[1] independent of the orientation of the bounding grains [14]. IGF absent (dry

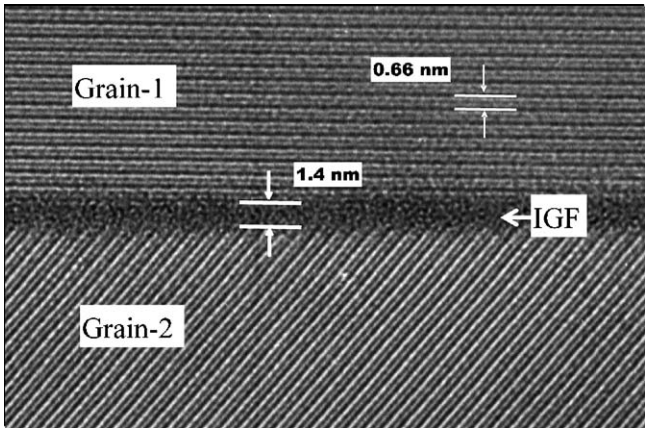

Fig. 2. High-resolution micrograph from a Lu–Mg doped Si_3N_4 sample showing the presence of an intergranular glassy film.

[1] Further comments on this point will be made later in the article

boundary) for low angle and special grain boundaries [15–17]. The surface film counterpart of the dry boundary also exists [18].
- Dependent on chemistry (Section 4.1.2).
- Independent of amount of glass, the excess glass goes to the triple pocket/excluded from the IGF [19].
- Crystallization of the glass by heat treatment does not get rid of the IGF (Section 4.2.6).
- Composition and atomic structure of the glass in the IGF is different from the bulk glass [10,20].
- Basic requirements for IGF to form:
  - bulk liquid should not be fully wetting the grains;
  - non-zero dihedral angle at the point of contact of IGF and triple pocket (TP) contact angle.
- Important parameters with respect to IGFs: thickness of the film (or the full width half maximum in case of diffuse interfaces), Structure of the film (any ordering, preferential segregation, etc.), temperature, pressure, chemistry, orientation of the bounding grains (crystallography). The principle goal would be the design of phase diagrams that include the microstructure in addition to the classical parameters:

$$\text{phase} = f(\text{temperature, pressure, chemistry, crystallography, IGF thickness})$$

2. Transmission electron microscopy [21]

Starting with the pioneering work of Clarke [22] transmission electron microscopy (TEM) has continued to be the major tool in the study of IGFs. Additionally, Auger electron spectroscopy [23,24], impedance spectroscopy [25,26] and mechanical spectroscopy [27,28] have also proved to be useful techniques for characterizing the grain boundary region. While scanning electron microscopy (SEM) on plasma-etched polished surfaces, of IGF containing materials reveals their presence, higher resolution is required for their detailed investigation.

Important advances have been made in the technology of microscopes, which have made it an invaluable tool in the study of materials [29]. These include: (i) spherical aberration correctors for illumination as well as imaging lens systems, (ii) electron beam monochromators reducing the energy spread of the electron beam to <0.1 eV, (iii) high-energy resolution spectrometers, (iv) imaging energy filters, (v) advanced specimen holders for in-situ experiments, (vi) high-sensitivity and high-dynamic-range detectors for images, diffraction patterns, electron energy loss spectra (EELS) and energy dispersive X-ray spectra (EDXS). The use of new methods, such as focal series reconstruction has added to its utility. Thus, it has become possible to record phase contrast images with point resolutions of well below 0.1 nm, or alternatively, scan electron probes of size <0.1 nm across the specimen, recording high-angle scattering or high-energy-resolution spectra from areas as small as a single atomic column.

In this section the utility of various TEM techniques in studying IGF structure is briefly outlined leaving out the details of the techniques. Emphasis has been given to references which compare the various techniques for the study of IGFs.

2.1. High-resolution transmission electron microscopy (HRTEM) [30]

This technique, using lattice fringe contrast produced by the periodic structure of crystalline material, has proved to be the definitive method for the measurement of film thickness. If the interface is diffuse an underestimate of the film thickness may be obtained by HRTEM [31]. Using a focal series reconstruction of the complex exit-face wave function, different groups [32,33] have detected order induced by the Si_3N_4 grains, on the material of the IGF adjacent to it. While this technique may be used to remove image aberrations giving rise to the delocalization of image features such as the exact position of interfaces; it does not remove the effect of plural electron scattering, being a major hurdle in the straight-forward interpretation of HRTEM images. Some of the important points regarding the technique are:

- accurate measurement of the film thickness can be made;
- the grain boundary needs to be exactly edge on;
- the GB needs to be straight, i.e., width of projection = width of film;
- cumbersome and hence difficult to analyze large number of boundaries.

2.2. Analytical electron microscopy (AEM)

Energy-dispersive X-ray spectroscopy (EDXS) and electron energy loss spectroscopy (EELS) are important tools in the study of interfaces [34]. While spatially resolved EDXS, detecting X-rays produced during inelastic scattering events of electrons passing through the specimen, requires a fine probe to be scanned over the sample, imaging energy filters may be used to form images using only those electrons having lost a certain amount of energy, in which case it is called energy-filtered TEM (EFTEM). Imaging energy filters may also be used to simultaneously record spectra integrated along one spatial dimension on the sample [35], but separated along the other (electron energy-loss spectroscopic profiling)—a very elegant way to record EELS line scans across straight interfaces in a single exposure, especially, if radiation damage and/or specimen contamination are a concern.

EELS has provided details of the distribution of chemical species across the grain, triple pocket and the film [36]. Comparison of the chemical width (the extent of distributions into the bounding crystals) with structural width of the film shows, that the former gives a larger value for the thickness [37]. EELS using energy loss near edge structure (ELNES) has been used to quantify GBs on a sub-nanometer scale. Gu et al. [38] used ELNES features as an aid to subtract the grain contribution from a mixed grain and GB signal, obtaining the signal representative of the GB alone.

2.3. High-angle annular dark-field scanning TEM (HAADAF-STEM)

With the resolution of HAADAF scanning transmission electron microscopes already reaching below 0.1 nm, it is now

possible to take advantage of the good sensitivity (of electrons scattered to high angles) to the atomic number and image the segregation of rare-earth elements in the IGF, to the grain interface [39,40].

2.4. Diffuse dark-field (DDF) imaging

This comparatively simple technique, in which images formed with an objective aperture placed over the diffraction rings produced by the amorphous material (but between diffraction spots produced by the crystal), reveal the presence of IGFs. The thickness measured using DDF is usually larger than that determined by HREM [30], which may, in part, be due to the spatial resolution limiting objective aperture.

2.5. Off-axis electron holography [41]

By interfering the scattered electron wave with a reference wave (passing through vacuum), the phase-shift introduced by the projected mean inner potential, as well as magnetic fields present in the specimen, can be measured. For most systems of interest to the study of IGFs, the magnetic contribution may be neglected, so that phase shifts across the interface may be interpreted in terms of: (i) grain boundary grooving due to preferential thinning of the amorphous material during final TEM specimen preparation steps, (ii) changes in chemical composition and/or density and (iii) accumulation of space charge. While analytical microscopy may help to separate the chemical from the space charge contribution, the exact knowledge of the mean free inelastic scattering path length for the local chemical composition and structure must be known, in order to determine the local thickness and thus the amount of grain boundary grooving.

2.6. Fresnel fringe method [42,30]

The thickness of the IGF can be determined by fitting model GB electrostatic potential profiles, to a series of images recorded at different (rather large) defoci, showing strong Fresnel contrast [43,44]. When assuming a step-like shape of the GB profile, the value of the thickness determined by this technique is about 20–35% more than that determined by HREM [30]. The mean inner potential profile of the interfaces can also be obtained directly from the Fresnel through focal series [45]. Grooving of the interface (IGF), at the top and bottom of the specimen during ion milling (TEM specimen preparation), can lead to different thickness at the GB region, which could be mistaken for an altered potential at the GB. Since the Fresnel Fringe method is an inline holographic method, it is, apart from its inability to retrieve very low spatial frequency information, an alternative to off-axis holography.

2.7. Diffraction

2.7.1. Diffraction streaking

In order to avoid the blurring effects of lens aberrations involved in the formation of images, the scattered electrons may be recorded directly. This takes advantage of the fact that the scattering of straight interfaces is condensed into a single streak in the diffraction pattern. Data interpretation is not as straightforward as for images and requires either fitting of parameterized model structures [46–48] or some direct method for solving the phase problem.

2.7.2. Imaging segregation by diffraction

Fourier transform of electron diffraction patterns, from a sample region containing an interface, can reveal the presence of atoms segregated to specific sites with respect to one of the grains [49]. This is due to the fact that dynamic electron scattering effects are very sensitive to the atomic number.

2.7.3. Radial distribution function

It is now possible to obtain diffraction patterns form small volumes of amorphous material [50]. Using a convergent probe focussed on the IGF, Döblinger et al. [51] performed electron diffraction experiments to obtain its reduced radial distribution function, giving information about the local atomic structure. A similar analysis may also be performed using the complex exit-face wave function reconstructed from a through focal series of images or off-axis holograms [52].

2.8. Beyond projection: three-dimensional (3D) TEM

In addition to limitations imposed by energy and spatial resolution of current instrumentation; none of current techniques (be it single TEM images, the reconstructed complex exit-face wave function, or spectroscopic data (e.g. EELS/EDXS spectra, EFTEM series)) gives us information in the dimension of the sample that is parallel to the electron beam. The following provide an exploration into the third dimension.

2.8.1. Optical sectioning using an aberration corrected STEM [53]

Recently developed aberration corrected STEMs are able to focus electrons to a cigar-shaped probe of width <0.1 nm and only a few nanometre long. By changing the focus of the probe forming lens, a two-dimensional EELS, EDXS and/or HAADF-STEM scan may be extended to a three-dimensional one, although with limited resolution in z direction (the dimension parallel to the electron beam).

2.8.2. Tomography of holographic, spectral and HAADF-STEM data [54]

Tomographic reconstruction algorithms can reconstruct 3D objects from a set of two-dimensional (2D) projections, recorded at different sample orientations, by solving a set of linear equations. These algorithms require that each of these 2D data sets (images, elemental maps, mean inner potential maps) is monotonic in specimen thickness, which is, due to multiple electron scattering, usually not the case for HRTEM images. On the other hand, the local mean inner potential observed by off-axis holography, EELS and EDXS spectral data and the HAADF-STEM signal [54], satisfy this condition for moderate specimen thicknesses, so that tomographic reconstruction algorithms can be applied to them. It is also conceivable to reconstruct the 3D shape

of the amorphous film, by applying tomography to the complex exit-face wave function, from which the crystalline contribution has been removed by the use of proper Fourier filtering methods. Such an analysis would finally be able to distinguish between rough grain/IGF interfaces (featuring islands of the grain protruding into the IGF) and genuinely diffuse ones.

The resolution-limit in the third dimension is determined by the order of electron lens aberrations being corrected for in the case of optical sectioning, or the specimen and specimen holder geometry defining the maximum tilt angle for tomographic experiments. In most cases the resolution normal to the sample surface will be much less than that in the plane of the thin TEM specimen foil. However, a resolution of about 5–10 nm is already sufficient to extract the volume contribution to the projected data from surface ones, thus overcoming a major drawback of conventional TEM methods, which suffer from observations skewed by surface effects.

3. Approaches to understanding IGF: theoretical and computational advances

The different ways of looking at IGFs and various theoretical models to understand them are shown in Fig. 3. In addition to the models described in this section, the work of Brada and Clarke [55], Yoshiya et al. [56], Choi et al. [57] and Golczewski et al. [58,59] may be consulted.

3.1. Force balance: film thickness

The pioneering work of Clarke [60] was a significant motivating force towards the understanding of the formation of IGFs. In his model attractive force (van der Waals dispersion force) balances the repulsive force (structural disjoined force related to the distortion of the SiO_4^{4-} tetrahedra), which give rise to an equilibrium thickness for the amorphous film (∼1–2 nm). Further modifications to the model were made to include the contribution of an electrical double layer [61]. Dry boundaries were explained by Clarke as low energy configurations of either small angle GBs or special boundaries (seen as cusps in the interface energy versus misorientation plot) [16]. These cusps occur close to misorientations corresponding to coincidence site lattice (CSL) boundaries. The essence of the Clarke's model is summarized in Fig. 4. The energy criterion for the formation of IGF can be written as $2\gamma_l \leq \gamma_b$ (where γ_l is the glass-crystal interfacial energy and γ_b is grain boundary energy). To summarize:

- repulsive forces balance the attractive forces to give an equilibrium thickness for the film (∼1–2 nm);
- orientation effects of the grains are ignored in the model;
- dry boundaries are explained in terms of an interfacial energy criterion.

As Clarke's model has proved to be an important one in the study of IGFs and is based on the theory of colloids, a few points summarizing the results from colloid and surface science would be useful here [62,63]:

- Forces in colloidal systems include: electrostatic double layer, London dispersion, packing, long-range attractive, short-range repulsive, undulation, depletion and steric forces.
- Balance between attractive and repulsive forces can give rise to stable colloidal dispersion. Potential energy-separation curves with secondary minima can occur.
- Repulsive forces (disjoining pressure) can exist at high-electrolyte concentration, independent of any electrostatic contribution.
- Colloids can undergo reversible (flocculation) and irreversible (coagulation) particle associations.
- Colloids can form many phases: crystalline solid, isotropic liquid, gas, plastic crystals, amorphous solids (glasses), liquid crystals and gels.

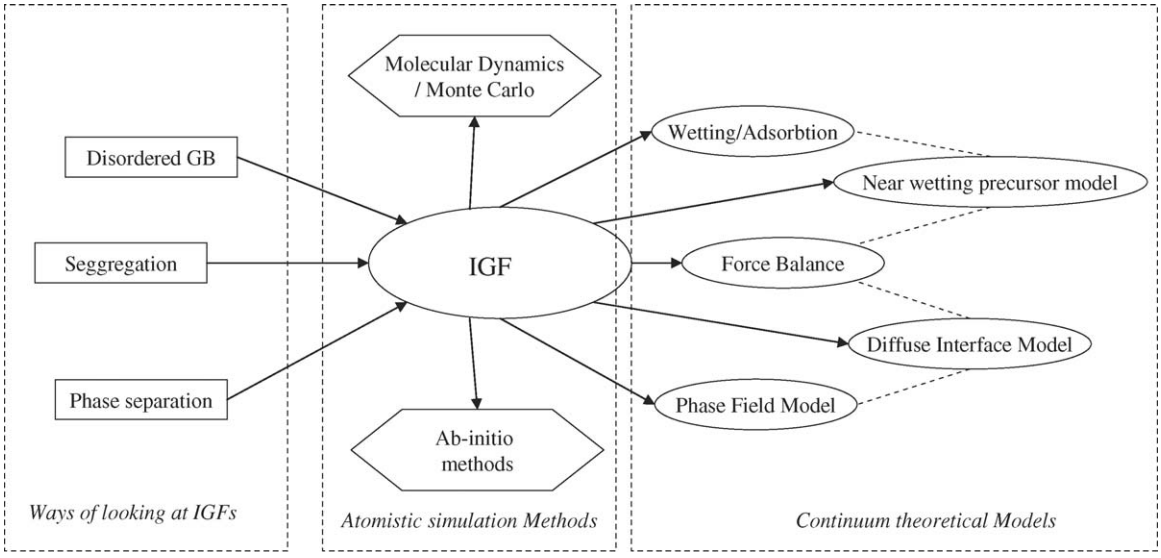

Fig. 3. The different ways of looking at IGFs and the theoretical models which have been used to understand them. References are in the text.

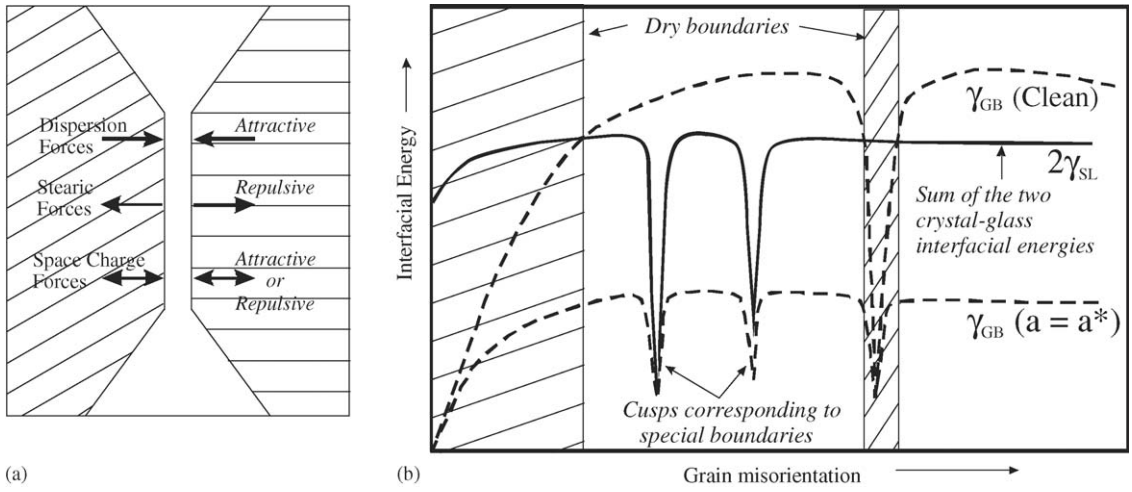

Fig. 4. Clarke's model: (a) forces leading to equilibrium, (b) explanation of dry boundaries based on interface energy versus misorientation plot. The hatched dry boundaries are based on γ_{GB} (clean). The γ_{GB} ($a = a^*$) corresponds to the GB energy with adsorbate coverage at an equilibrium concentration, appropriate to the two phase co-existence condition [71].

3.2. Diffuse interface model: graded composition of the film

There are two important extensions to Clarke's force balance theory based on the idea that the crystal-IGF interface may be diffuse and not sharp.

3.2.1. Modification of Ackler and Chiang [64,65]

Ackler and Chiang [64,65] via improved treatment of the liquid structure based on the diffuse interface theory of Cahn and Hilliard [66], have predicted that liquid structure alone can result in attractive as well as repulsive interactions. The essence of the theory is that the crystal surface imposes an order on the liquid adjacent to it and there exists an interface region where the order is in between that of the liquid and the crystal [32]. Modifying the parameters in the theory the investigators show, that the behaviour predicted by Clarke's theory with a single minimum in the energy–displacement curve and a situation with two minima (one at zero displacement separated with the other minima at finite displacement by a steep barrier) are both possible (Fig. 5). If the two minima situation exists in any system then liquid will not penetrate an already dense polycrystal immersed in glass (refer Section 4.2.1). In summary:

- crystal imposes an order on the adjacent liquid leading to a transition in order of the crystal to the disorder in the liquid;
- based on the liquid structure alone attractive and repulsive interactions can result;
- depending on the relative values of the parameters in the theory a situation with two minima in the energy–displacement curve is predicted with a strong barrier separating the two minima;
- a decrease in the film thickness is predicted with an increase in temperature.

3.2.2. Approach of Bobeth et al. [67]

With subsequent research after Clarke's model was proposed, it was realized that the composition of the IGF may not be uniform and the glass crystal interface could be diffuse rather than sharp. Bobeth et al. [67] proposed a thermodynamic diffuse interface formalism based on the formulation of Cahn and Hilliard [66], in which, equilibrium exists between a multilayer of liquid and solid phases. They found that when the thickness of the liquid approaches a characteristic length scale (the interface width) then its composition can deviate markedly from the bulk liquid phase composition. An important conclusion from this work is that in the presence of purely chemical interactions, a thin film of liquid in contact with a reservoir would go thinning and would vanish. Existence of IGFs thus implies that other forces (repulsive structural and electrostatic forces and attractive van der Waals forces) must exist.

3.3. Adsorption/segregation/wetting approach [68–71]

The wisdom gained from research in the areas of segregation and wetting can be applied to the understanding of IGFs. Start-

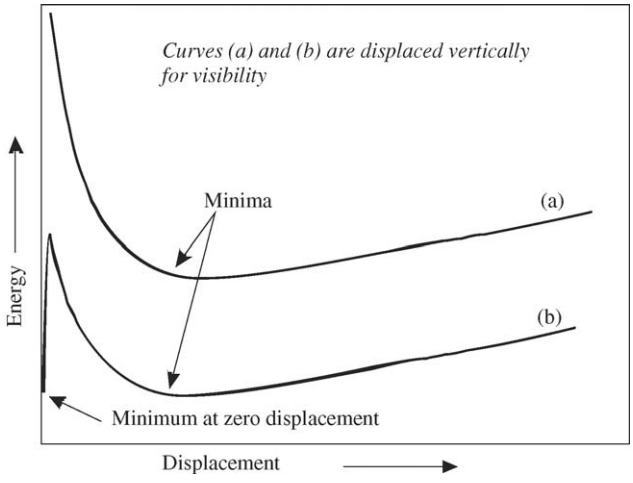

Fig. 5. Schematic representation of two possible energy–displacement curves leading to equilibrium thickness of film: (a) with one minimum in the range of a nanometer separation (Clarke's model); (b) with two minima separated by a strong barrier (modification of Ackler and Chiang to Clarke's model).

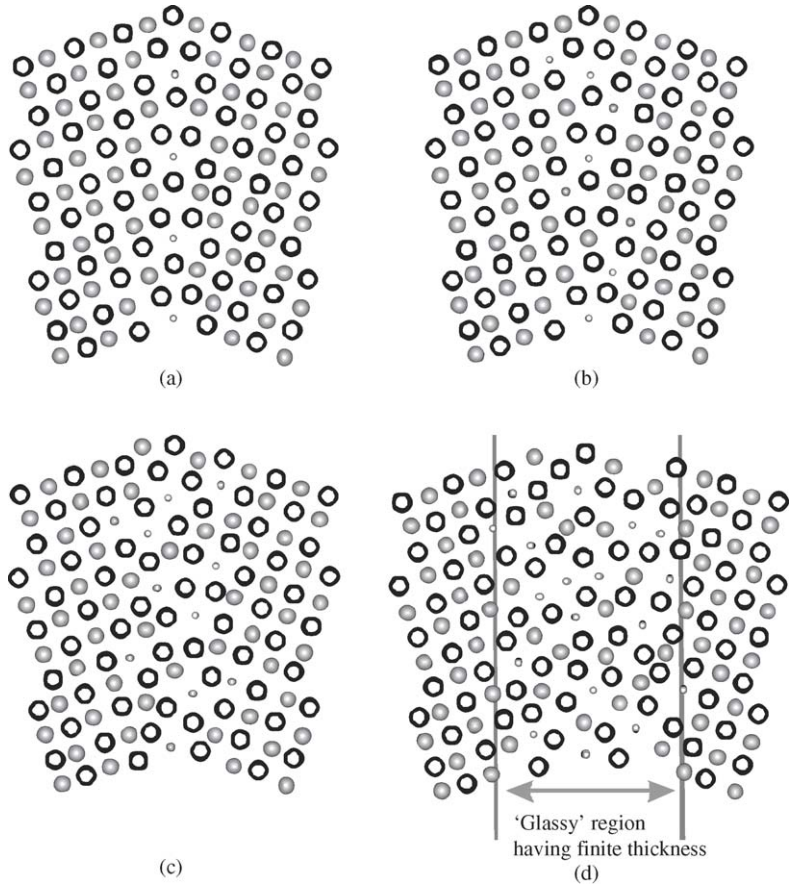

Fig. 6. Progressive addition of a species preferentially segregating to a grain boundary: (a) monolayer, (b–d) multilayer. The representation in (d) is close to that of an IGF (i.e. a separate amorphous film).

ing with a sub-monolayer coverage, segregation can increase to a multilayer configuration, followed by a complete "wetting" of the GB (Fig. 6). From this point of view IGFs can be classified as graded multilayer adsorbates. The word graded has been used to describe the diffuse nature of the crystal-glass interface. The effect of space charge on the segregation has also been considered in the framework of segregation theories. Prediction of the structure of the GB as a function of the temperature and activity of the adsorbate species is an important goal of these models. From the point of view of wetting, IGFs can be considered as partially wetting or prewetting films. These theories, though still in there early days, have been able to qualitatively describe certain features of IGFs, like their equilibrium thickness and temperature dependence.

3.4. Phase-field model [72]

The homogeneous free energy of a non-uniform system depends in addition to the usual parameters such as composition, structure, electrostatic potential, density, etc., also on their gradients, i.e., their deviations from uniformity. Steep gradients present at abrupt interfaces become therefore energetically "expensive", causing such interfaces to become diffuse. Since these gradients do not exist in bulk material the energy penalties associated with them must be determined from atomistic simulations [73] and by fitting phase-field simulation results to careful experiments performed on the amorphous films themselves. The applicability of any such continuum model depends on how accurate the physics determining the thermodynamic quantities of the system is described. In the Kobayashi–Warren–Carter model [74], for example, the energy penalty for changing the structural orientation is lowered in the presence of disordered material, so that amorphous boundaries will be more likely to occur at large-angle grain boundaries than small angle ones, which is in agreement with experimental observation (see Fig. 4b). Expanding this model, Bishop has recently shown [72] that it is possible to predict many trends expected by such systems in response to changes in composition, temperature, etc. This model allows the exploration of large "volumes" in phase-space and even dynamical processes which are not accessible to the computationally more expensive atomistic methods, yet.

3.5. Classical density functional approach

Classical density functional theory (CDFT) minimizes the Hemholtz free energy, which in turn is a function of the local number density (number of atoms of a certain atomic species per volume) of the various chemical species and has been developed for solid-liquid interfaces in the 1970s and 1980s. By treating the number density as a continuous quantity it provides a rigorous link between atomistic models of IGFs and continuum phase-field models [75]. The reciprocal space representation of the

number density, called the structure factor, may be determined from electron- or X-ray diffraction experiments [46], providing also a direct link between theory and certain experiments.

3.6. Molecular dynamics (MD): atomic structure

Describing an IGF with (continuum) models rests on the assumption of selected physical processes dominating its behavior. Molecular dynamics (MD) calculations provide a way to build atomic IGF models just from an accurate knowledge of the forces between the atoms and the thermodynamic boundary conditions of the finite sized system. Using this technique Keblinski et al. [76] have investigated the tendency of a one-component system (Si, for which inter-atomic potentials are well established) to form amorphous films at different Σ-type grain boundaries, confirming the existence of a grain boundary energy threshold above which IGFs form, but below which the Read–Shockley model of grain boundary energy relaxation by means of local relaxation along dislocation cores proved to be valid. However, the experimental verification of the existence of IGFs in silicon has not been successful yet.

For ceramics, Garofalini et al. have been able to study the segregation of cations (Ca^{2+}) to either the edge (in alumina [77]) or the center (in silicon nitride [78]) of the calcium silicate IGFs, increasing or weakening the strength of the films respectively, but weakening the interface in both cases for larger amount of CaO present in the film. The authors point out that the existence of equilibrium width IGFs may be related to this concentration dependent strength of the interface in the case of Si_3N_4 [78]. In addition, the periodic crystal potential may induce special periodically arranged atomic configurations next to the crystal/IGF interface [79], producing a so-called Stern layer.

3.7. Grand canonical Monte-Carlo (MC) methods

Intergranular films in ceramics are two-grain junctions terminated by much thicker multi-grain pockets which may be of different compositions than the films. The number of atoms of a given species with a certain IGF volume may therefore not be determined from the amount of additives forming the ceramic. Within certain limits the IGF may actually "select" its composition from the large pool of atoms present in the pockets. While molecular dynamics methods generate atomic configurations by solving Newton's equation of motion for a given number of atoms within the simulation volume, Monte-Carlo methods consider the correct statistical mechanics ensemble, which, in the case of an "open" system with infinite atom reservoirs is the grand canonical ensemble. This means that atoms are not only allowed to change their position in response to the force-field created by atoms surrounding it, but may also change their type in response to the local chemical potential (see [80] for a recent review).

However, although this approach seems to describe the boundary conditions of intergranular films more accurately than molecular dynamics, the fact that the IGF width still depends to some degree on the amount of sintering additives suggests that the finite size of the pockets and the amount of atoms of a certain species left in the "reservoirs" does have an influence on the IGF system to be modeled.

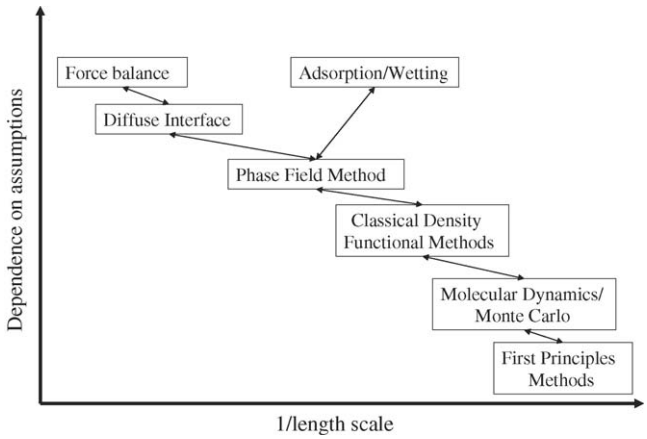

Fig. 7. Evolution of various models starting from Clarke's model.

3.8. First-principles methods

First-principles, or ab-initio methods use only fundamental quantum-mechanical principles and quantum mechanical density functional theory [81] to calculate the total energy of a system and are therefore considered more rigorous but also require much more computing power and time than all of the more approximate methods just mentioned. Their application to IGFs is limited due to the large number of atoms required to accurately describe amorphous structures and the correct boundary conditions confining them. While MD, MC and continuum models may be used to simulate dynamic processes at elevated temperatures, this method is usually limited to 0 K temperature. In the context of amorphous IGFs it has been proven very useful to calculate certain atomic configurations, such as favorable segregation sites of rare-earth atoms [39], stable crystalline phases formed by IGF constituents [82], but also the relaxation of whole IGF atomic models obtained by MD [83]. In addition to the atomic structure this method delivers information about the electronic band structure of the system which may then be used to simulate electron energy loss spectra (EELS) [84] as they would be observed in an electron microscope.

3.9. Comments

Starting with Clarke's model a smooth transition can be seen to some of the other models mentioned in this section (Fig. 7). Approaches like the near-wetting precursor model [70] have also been put forth which combines the wetting and force balance analysis of IGFs.

4. Important experiments and lessons

In this section we summarize various important experiments leading to the formation of IGF and the effect of various stimuli on IGFs. A gist of the experiments in this section, summarizing the principal methods of formation of IGFs (and surface films)

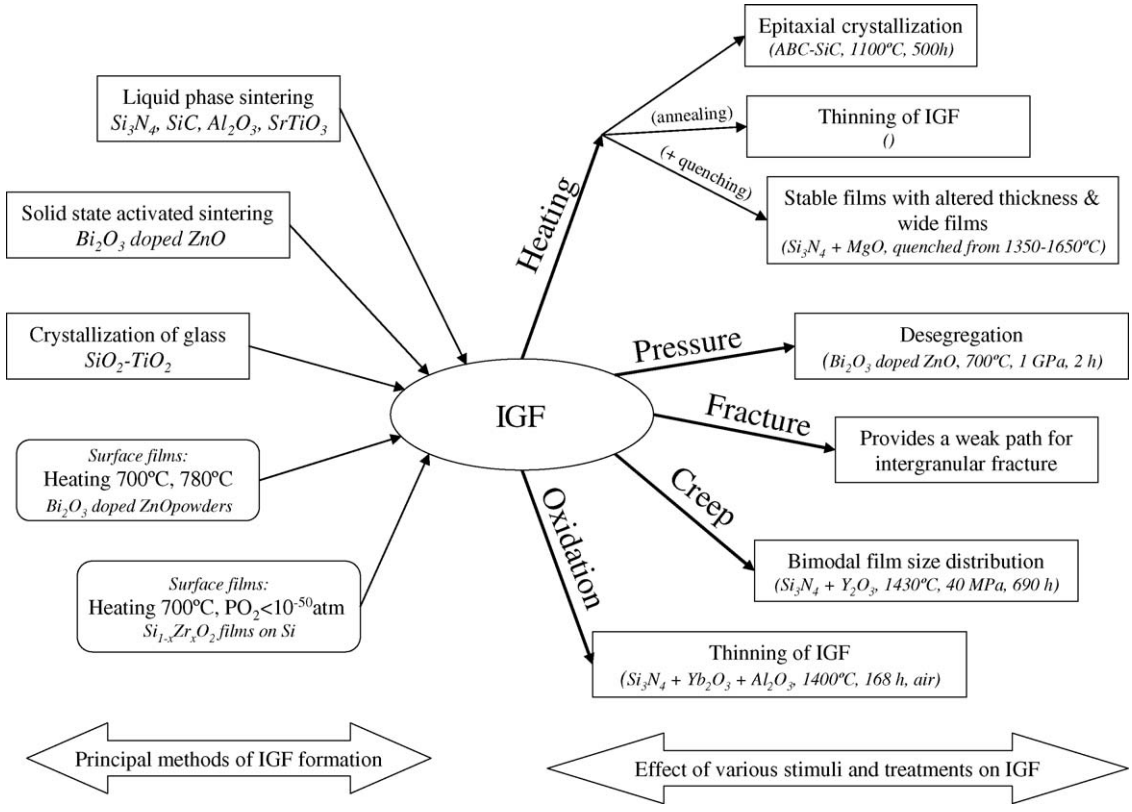

Fig. 8. Principal methods for the formation of IGF and surface films and the effect of various stimuli and treatments on the evolution of IGFs. References are in the text.

and the effect of various stimuli and treatments on the evolution of IGFs is shown in Fig. 8.

4.1. Formation, chemistry dependence and structure

Conventionally IGFs are formed in systems like Si_3N_4 and SiC, by liquid phase sintering the starting powder with additives. For Si_3N_4, it requires special conditions, e.g. high-purity undoped starting material and processing by CVD, to avoid the formation of IGF in a random grain boundary [1]. In the case of the liquid phase sintered ceramic, the IGF can be perceived as the remaining liquid which is kinetically frozen; but this is a rather restrictive point of view in understanding these films (as seen regarding their structure in Section 2.1 and from synthetic methods described in this section).

4.1.1. Importance of starting configuration

In Si_3N_4 and ruthenate systems an amorphous film covers the particles before sintering to a dense material and this feature is not found in systems like Al_2O_3 and $SrTiO_3$. Hence, it is interesting to note that how these films form from different starting points and different processing routes.

Experiments in the TiO_2–SiO_2 system have shown that the starting configuration could be important. Ackler and Chiang [65] in a neat experiment in the TiO_2–SiO_2 system, studied the approach to equilibrium configuration from two directions: (i) from grains initially in contact and (ii) from grains separated by a thick amorphous film. Their experiments showed if the grains are initially in contact then they are not penetrated by glass and if they are separated by a glass film (obtained by a coating of SiO_2 on TiO_2 particles), then they approach equilibrium thickness of about 1.5 nm. This result was explained in terms of two minima in the energy–distance curve (at zero separation and at the usual equilibrium separation) separated by a strong barrier (Section 3.2). Further experiments of this type are described in Section 4.2.1.

- Depending on the system the starting configuration could play a crucial role in the formation of IGF.

4.1.2. Dependence of thickness on chemistry

4.1.2.1. Ca doping in Si_3N_4. The thickness of the IGF is found to be a sensitive function of the dopant concentration and type of dopant. Tanaka et al. [85] systematically doped various amounts of Ca (0–450 at. ppm) to Si_3N_4 and found that the thickness of IGF decreased in the dilute region (<80 ppm of Ca) but then increased with further additions of Ca. The result was explained by the investigators in terms of Clarke's theory [61] including electrical double layer forces.

4.1.2.2. Doping with lanthanide oxides. Wang et al. [19] densified Si_3N_4 with Y_2O_3 and various lanthanide oxides (La_2O_3, Nd_2O_3, Gd_2O_3 and Yb_2O_3) and found that the film thickness increased with increasing ionic radius of the lanthanide. A schematic illustration of the dependence of the thickness of the IGF on Ca and oxide additions is shown in Fig. 9a and b.

- Thickness of IGF is dependent on chemistry.

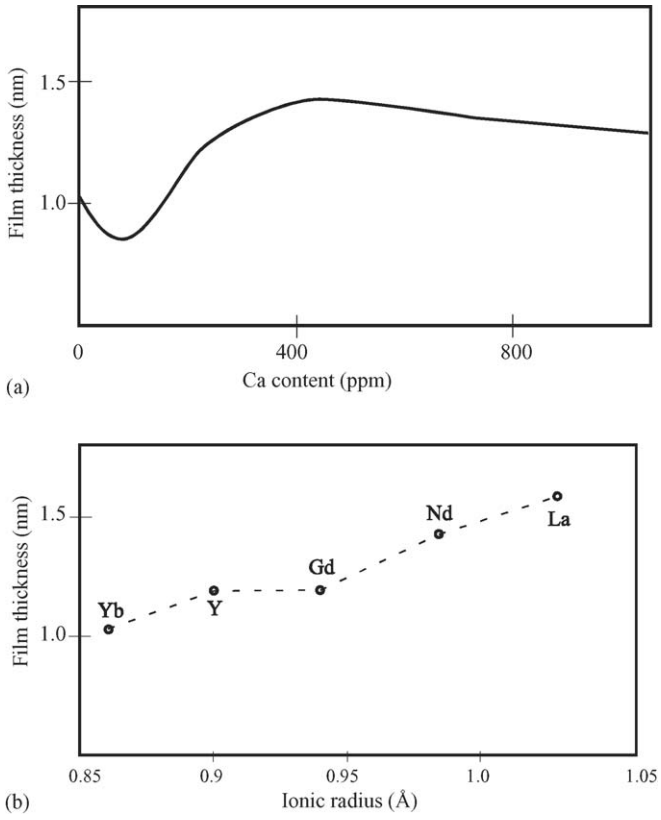

Fig. 9. Schematic showing dependence of IGF thickness on chemistry in Si_3N_4: (a) Ca content; (b) addition of oxides of Yb, Y, Gd, Nd and La.

4.1.3. Films from sub-eutectic sintering

As mentioned before, IGFs often form during liquid phase sintering it is easy to visualize them as the liquid remaining between grain boundaries after the system is frozen by cooling. From this simplistic point of view it is startling to note that IGFs can form from solid-state activated sintering, as observed in the Bi_2O_3 doped (~0.6 mol%) ZnO [86]. In this case the sample was densified from the doped powder by hot-pressing at 700 °C for 2 h under 1 GPa pressure, followed by annealing at the same temperature under 1 atm pressure for 24 h; thus carrying out the entire process below the eutectic temperature (of 740 °C). The IGFs thus formed have a ZnO rich composition which is different from that of the eutectic liquid [86].

- 700 °C (2 h, 1 GPa pressure + 24 h, 1 atm pressure) → IGF

4.1.4. Formation of films in flocculated Si_3N_3 crystals in a glass matrix

It is seen that Si_3N_4 particles dilutely dispersed in lanthanide-based glass flocculate into isolated clusters of about 3–5 particles each [19]. Larger clusters in striking flower like patterns are found in dispersions in La based glasses [87]. The important observation is that not only do IGFs form between the particles in the cluster but also that the thickness of the films are similar to that observed in the bulk polycrystalline counterparts. Additionally this configuration is close to that observed in colloids, which have been the inspiring force for Clarke's theory [60] (Section 3.1).

- IGF form in flocculated clusters of crystals in glass of thickness similar to that in a polycrystal.

4.1.5. Crystal growing from a melt to attain equilibrium thickness

Ackler and Chiang [8] deposited a thin SiO_2 film on a single crystal TiO_2 substrate, annealed this system to form a eutectic liquid in equilibrium with the substrate and then quenched the system to retain a amorphous layer on the TiO_2 crystal. The amorphous layer was crystallized to form a hetero-interface amorphous film about 1.5 nm thick. This geometry is free of residual stresses [88] and capillary effects [89] which have been envisaged to be kinetic impediments to complete crystallization.

4.1.6. Surface films

4.1.6.1. Bi_2O_3 films on ZnO. Bi_2O_3 doped ZnO powders were heated above (780 °C) and below (700 °C) the eutectic temperature to form amorphous surface films about 1.5 nm thick by Luo and Chiang [18]. Films form on the $\{1\,1\,\bar{2}\,0\}$ surfaces but, the $\{1\,\bar{1}\,0\,0\}$ surface was found to be free of the amorphous film (this would be the dry boundary counterpart of dry GBs in special cases). Further such films were observed in other systems as well (Bi_2O_3–Fe_2O_3, WO_3–TiO_2) and understood to be films in thermodynamic equilibrium [90].

4.1.6.2. $Si_{1-x}Zr_xO_2$ films on Si [91,92]. Using a closed system approach Chiang and his team at MIT grew nanometer thick oxide films ($Si_{1-x}Zr_xO_2$) on pristine silicon surfaces using non-stoichiometric oxides as source of oxygen and dopant cations. Very low level oxygen activity ($<10^{-50}$ at 700 °C) needs to be maintained to prevent bulk oxidation.

- Surface films analogous to IGF of equilibrium thickness can be synthesized.

4.1.7. Segregation of RE to the interface

It was progressively realized that the composition of the film is different from that of the bulk glass found in the pockets. In β-Si_3N_4–SiO_2 system there is nitrogen excess in the IGF and composition lies in the miscibility gap [70]. The distribution of certain dopants between the glass in the pocket and the IGF is also different [36]. Further, the distribution of the dopant atoms within the film is also not uniform. These distributions are schematically represented in Fig. 10. The segregation of rare-earth elements to the interface has been characterized by HAADF [39,40] and captured by first-principles atomic cluster calculations [39]. Additionally, segregation of Ca has been observed in MD simulations [77]. On the other hand interfacial segregation of anionic impurity like fluorine is not expected [1].

- Certain cations selectively segregate to the IGF–crystal interface.

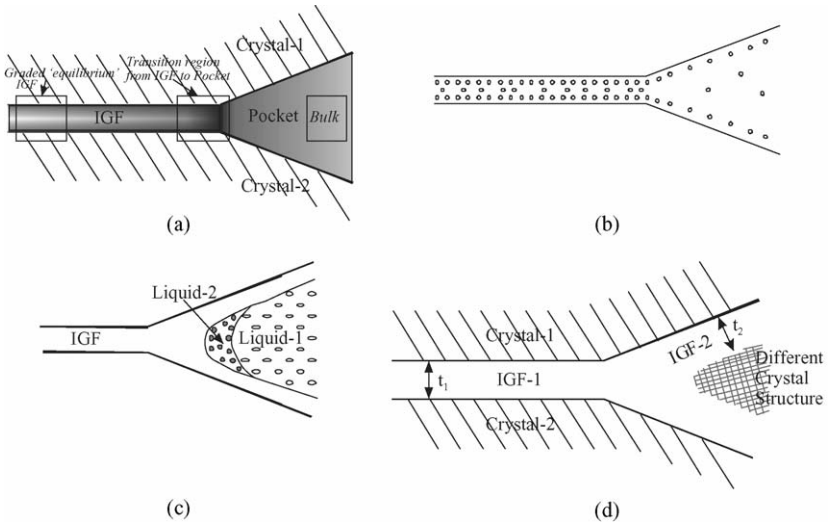

Fig. 10. Illustration of various possible triple pocket (TP)-IGF configurations: (a) schematic of the TP-IGF region, (b) segregation of Ca, (c) phase separation of the TP glass, (d) formation of crystalline phase in the TP giving rise to a heterophase IGF.

4.1.8. GBs in metallic systems

Parallel with the literature in ceramic systems on IGFs, there is a considerable body of knowledge gained via studies of segregation in metallic systems [93,94]. Research on systems like Al–Sn, Al–Ga, Al–Sn–Ga, Cu–In, Cu–Bi, Fe–Si–Zn, Mo–Ni, W–Ni, Zn–Sn and Zn–In, show the existence of a variety of GB phase transitions, like wetting, prewetting, premelting, melting, faceting and special-random GB transition. This has led to the incorporation of lines of GB phase transitions into phase diagrams [93].

While, detailed high-resolution studies (of IGFs), usually found in the ceramic systems, are missing in their metallic counterparts, the temperature and activity dependence of segregation have been well characterized; especially in the Cu–Bi system [95]. Prewetting phase transitions in the Cu–Bi system can lead to the formation of about two monolayers of liquid like grain boundary phase. This phase is not stable in the bulk. The important result in this system is that: heating to a temperature in the prewetting region of the phase diagram (incorporating GB effects), leads to a reduced Bi coverage along the GB [96]. Alloys with prewetted layer along GBs show enhanced GB diffusivity of Cu and Bi (by about two orders of magnitude).

As illustrated before, multilayer disordered segregation (adsorbate) at GB can be visualized as an IGF and hence, based on the investigations in the metallic systems, there is sufficient reason to believe that, metallic systems also form structures analogous to IGFs.

4.2. Effect of various stimuli on the film thickness

4.2.1. Flocculation/deflocculation/penetration by glass

The existence of an equilibrium thickness film implies that, sintering of densified polycrystalline ceramic having an IGF, in the presence of a large quantity of glass will not alter the thickness of the IGF. This tendency to maintain a constant thickness is expected to depend on the temperature and the composition of the glass. Experiments have been performed in Al_2O_3 [97,98] and $ZnO–Bi_2O_3$ [99,100] systems to study the effect of penetration of glass into the grain boundaries of a dense polycrystalline ceramic. These experiments further throw light on the relative effects of attractive and repulsive forces and there range of interaction.

In the experiment of Chiang et al. [100], densified polycrystalline $ZnO–Bi_2O_3$ was immersed in a pre-equilibrated $ZnO–Bi_2O_3$ liquid (70 mol% Bi_2O_3) at 750, 850 and 950 °C for 24 h. It was observed that deflocculation occurred only at 950 °C. The authors have used a changing van der Walls force with temperature to explain their results. Given that the typical sintering temperature of this ceramic is greater than 1150 °C, the authors have concluded that the grains are stopped from separating at the sintering temperature by the limited fraction of liquid and the resulting capillary forces.

4.2.2. Long-time annealing: films become thinner

Annealing experiments carried out for 10,000 h show that IGFs become thinner [101]. In the creep experiments of Jin et al. [102] (1430 °C, 40 MPa, 690 h)) the uncrept grip end of the sample can be assumed to have undergone pure annealing. Comparison of the thickness of the IGF from this part of the sample with that in literature [1] (for a similar composition) leads us to conclude that annealing has lead to thinning of the IGF.

4.2.3. Heating followed by quenching

The formation and evolution of grain boundary films at high temperatures (at and below the sintering temperature), is of considerable importance towards understanding the basic science behind IGFs; especially from the point of view of their applications. High-temperature quenching experiments can give considerable insight into this domain [103–105]. Cinibulk and Kleebe [105] heated disc shaped specimens of Si_3N_4 (MgO fluxed and hot pressed) for eight temperatures between 1350 and 1650 °C for 5, 15 or 300 s and quenched them in water. The general trend seen is that IGF gets thicker (from 8 to 13 Å) with increasing temperature (from 1350 to 1650 °C); with exceptions

in the samples quenched from 1420 to 1500 °C, wherein the IGF becomes metastable (non-equilibrium) and increased (variable) film thicknesses are observed [105]. The steady increase in film thickness is understood as a change in equilibrium thickness of the film with temperature, while the non-equilibrium films are explained as occurring due to Si_3N_4 dissolution with hindrance to glass redistribution (leading to equilibrium) due to high viscocity [105]. These experiments need to be supplemented with further work which can give us a compete picture of the evolution of IGFs as a function of temperature (with accompanying change in chemistry), keeping in mind the kinetic factors.

4.2.4. In-situ heating

Clarke [103] had concluded from hot stage TEM experiments that changes to microstructure occur only above 1000 °C. Recent in-situ heating experiments in La and Lu doped Si_3N_4 [106,107] have shown surprising results, which are contrary to what was expected from the experiments of Clarke [103] and Cinibulk and Kleebe [105]. Alteration to the grain boundary thickness were observed during in-situ heating experiments in 1250, 400 and 120 kV microscopes at temperatures below 1000 °C [106,107]. A complete understanding of the results of these experiments has not been achieved yet.

- Complete understanding of the high-temperature behaviour of IGFs has not yet been achieved.

4.2.5. Oxidation: reduction in film thickness

Oxidation is expected to change the chemistry of the sample which in turn is expected to change the thickness of the IGF. Cinibulk and Kleebe [108] oxidized two samples of Si_3N_4 (at 1400 °C for 168 h): (i) Si_3N_4 with 5 vol.% Yb_2O_3 and 0.5 vol.% Al_2O_3 having a secondary crystalline phase and (ii) Si_3N_4 with 5 wt.% Y_2O_3 and 1 wt.% MgO with amorphous secondary phase. In both the cases they saw a reduction in the thickness of the film by about 20% from an initial value of about 1–1.2 nm. The authors have explained their result in terms of an inward diffusion of oxygen, with a concurrent outward diffusion of cations, leading to a changed chemistry, which influences the thickness of the IGF.

- Changes in chemistry due to oxidation (inward diffusion of oxygen+ outward diffusion of cations) leads to thinning of IGFs.

4.2.6. Crystallization of glass

The glass in the triple pocket can undergo phase separation and also crystallization [109]. It was found that crystallization of glass in the pockets can improve the high-temperature properties of Si_3N_4 [110]. However, it was realized that complete crystallization of the amorphous phase cannot be attained and residual glass remains at internal interfaces (IGF) [111]. The effect of internal stresses (due to volume change on crystallization) on the crystallization of intergranular phases has also been investigated [88].

- Epitaxial crystallization in ABC-SiC:

  Zhang et al. [112] heat-treated hot-pressed SiC with Al, B and C additions (ABC-SiC) at 1100 °C for 500 h in Ar, to discover that the grain boundary amorphous film (of <2 nm width) had epitaxially crystallized.

4.2.7. Pressure

Processing of Bi_2O_3 doped ZnO at 700 °C, 1 GPa pressure for 2 h led to desegregation of film material [86]. Annealing at ambient pressure (650 °C, 24 h) restored the 1–1.5 nm IGF.

4.2.8. Creep: leading to bimodal size distribution

The presence of the IGFs is anticipated to most adversely affect the creep behaviour of a ceramic; as the glassy phase would soften at high temperatures leading to enhanced creep rates. The experiments in Section 4.2.6 were aimed at crystallizing the amorphous phase to alleviate this problem. In this section we describe the effect of creep deformation on the IGF.

In the experiment of Jin et al. [102] multiphase hot isostatically pressed Si_3N_4 (with 4 wt% Y_2O_3) was subjected to tensile creep (1430 °C, 40 MPa, 690 h, with a total strain of 0.65%). Film widths which were uniform before creep showed a bimodal distribution after creep, which has been attributed to viscous flow of the boundary amorphous film material during creep by the investigators. The redistribution is expected to occur due to local normal stress at the boundaries. Wang et al. [113], in an earlier investigation on Si_3N_4 (with 5 wt% Y_2O_3, 2 wt% MgO), had superplastically deformed (1400–1500 °C, 40 MPa, to a total strain of −0.69%) the sample to obtain similar results.

4.2.9. Fracture behaviour [114]

By altering the composition and processing of the ceramic, the fracture mode can be altered to become intergranular from transgranular. Due to increased path length for the crack this implies increased fracture toughness. However, too weak a GB can lead to overall decrease in strength of the material and hence optimization is required. In the Si_3N_4 system, given that the strength of the bulk glass is similar to that of the ceramic, the occurrence of transgranular fracture implies that the IGF must have a weak plane which debonds leading to crack propagation. MD simulations of crack propagation have captured this aspect [77].

- Fracture studies suggest the existence of a “weak plane” in the IGF.

4.2.10. Testing in complex conditions: long time oxidizing creep

Creep fracture test of MgO sintered Si_3N_4 (commercially designated as NC-132) at 1100 °C in air for 14941 h using a pressure of 266 MPa led to the formation of depleted grain boundaries with no amorphous interlayer [115]. This experiment involves pressure, high temperature and an oxidizing environment and hence the results of the experiments are not that easy to interpret. The chemistry change involves inward diffusion of oxygen and outward diffusion of Mg from grain boundaries.

Large fraction of the depleted interfaces represented small angle grain boundaries.

5. Further points

5.1. Factors to be kept in mind while interpreting the results

Original interpretation of the authors has been provided for the experiments in Section 4. It is encouraged that the readers understand/reinterpret the results in the light of the growing body of knowledge.

In some of the experiments mentioned in Section 4, e.g. creep or in-situ heating there could be a combined effect of a given stimuli and change in chemistry which leads to the results observed. Hence, the following points should be kept in mind while interpreting the results of these and other experiments:

- change in chemistry (/loss of material) of (/from) either the entire sample or just the IGF;
- time of the experiment: given the time scale of some of the experiments the configuration seen could be kinetically frozen one and any comparison with equilibrated structures should be done carefully;
- thin-specimen effects in a TEM;
- electron beam irradiation effects in in-situ experiments in the TEM (the extent of damage being voltage dependent).

5.2. Rough versus disordered interface

Often when a disordered contrast is seen at the grain boundary region, it should be remembered that a combination of factors could be responsible for this:

(i) true disorder at the boundary (Fig. 11a);
(ii) formation of an IGF;
(iii) roughening at the GB (Fig. 11b) [116];
(iv) strain at the grain boundary due to presence of dislocations, etc.

It should be borne in mind that the difference between (i) and (ii) above is often a question of definition. Electron tomography techniques would prove to be very useful in differentiating

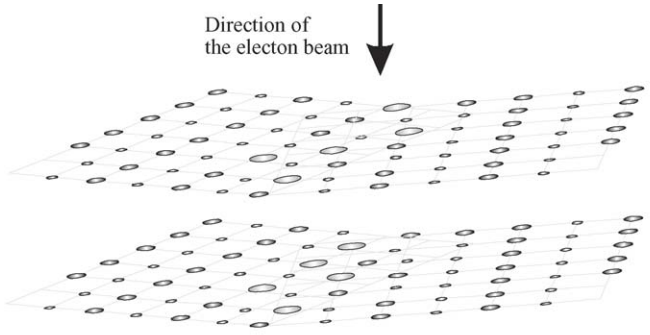

(a) Two planes in the path of the electon beam with differing order at the GB

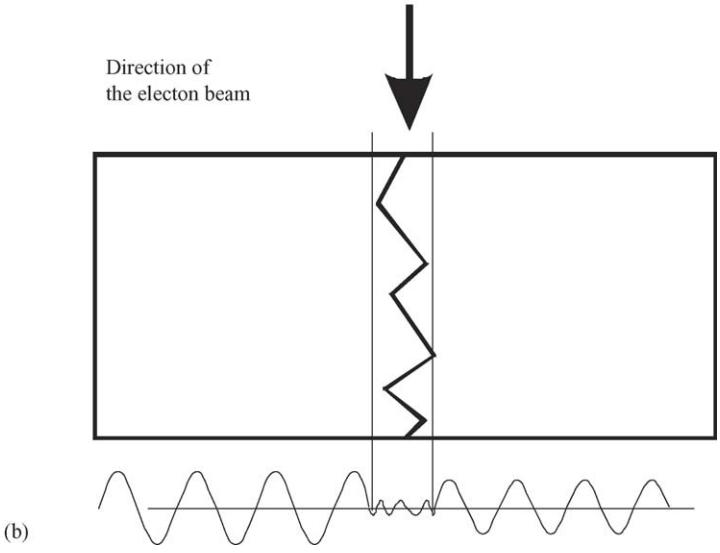

(b)

Fig. 11. Schematic illustration of: (a) two planes from a disordered boundary and (b) rough boundary. The ordering in (a) changes from plane to plane and is seen as amorphous contrast in the HRTEM. The rough boundary could be seen as a disordered boundary in a HRTEM. In reality the disorder shown in (a) extends into the third dimension as well.

between ordered rough interfaces and disordered straight interfaces.

5.3. Charge at the interface

The effect of space charge on the equilibrium film thickness has been dealt with by Clarke et al. [61]. Let us consider the case of a dopant atom of different valency than the grains of crystal segregated to the grain boundary. At absolute zero temperature the ion of the dopant atom (say positive charge) and the electron lost from the dopant atom are not dissociated and hence do not lead to any space charge. At higher temperatures due to entropic effects the electron can dissociate from the ion and migrate away from it leading to a net positive charge at the interface. Space charge has an important influence on the electrical properties of the ceramic (with IGFs), especially in ruthenate thick-film resistor materials [117,118] and ZnO ceramics [119].

5.4. Thickness

5.4.1. Thickness measurement

Some aspects regarding the relative merits of the various TEM techniques for thickness measurement were dealt with in Section 1 and some further aspects are considered here. By Fourier filtering the lattice fringes from the HRTEM image, MacLaren [31] has shown that a larger thickness for the IGF could be measured for the same boundary. Daschowdhury et al. [37], studying interface and grain boundaries in silicon nitride-silicon carbide whisker composites, showed that chemical widths are 10–120 times the structural widths. This ratio was larger for grain boundaries as compared to heterointerfaces. A schematic illustration of the various widths involved is shown in Fig. 12.

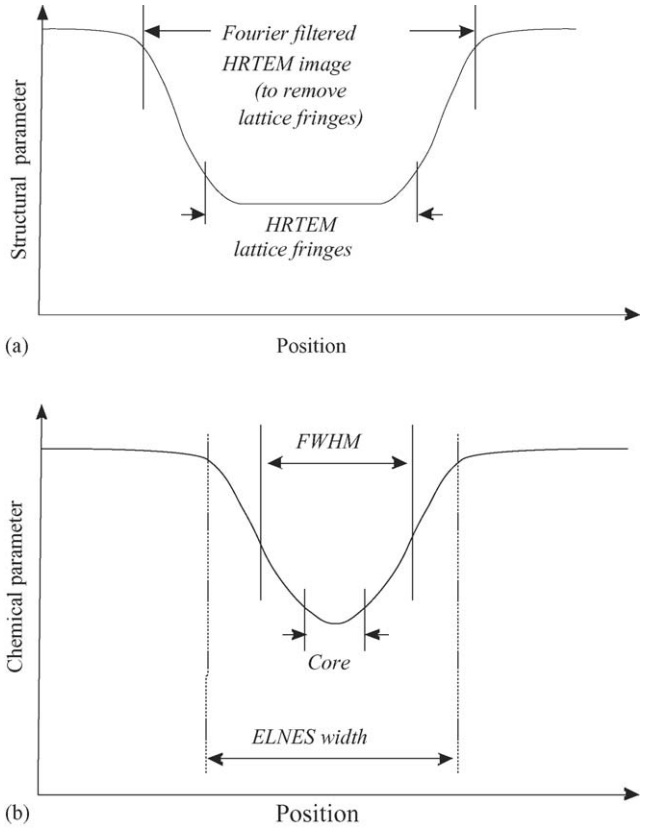

Fig. 12. A schematic comparison of structural (a) and chemical (b) widths of IGF. The position axis between (a) and (b) are not to scale. The core can be considered a region of constant composition with little gradients in structure or composition.

5.4.2. System dependence of the distribution of thickness

The deviation from the mean of the equilibrium homophase film thickness is system dependent. In the as-processed Si_3N_4 samples the thickness distribution is very narrow, which is different from the TiO_2–SiO_2, ruthenate and fine grained Si_3N_4 [120] systems [64].

5.4.3. Thickness of homophase versus heterophase boundaries

Earlier work by Kleebe et al. [14] had established the dependence of the film thickness on the composition of the sintering aids. They had added various rare-earth and transition-element oxide additions. The work also showed that, for the compositions studied, the heterophase films are thicker than that of homophase boundary films. Further work by Kleebe et al. [121] showed that the observed thicknesses fall within a narrow range of about 0.2 nm centered about a mean value.

5.4.4. Orientation of the bounding grains on the thickness of the IGF

Due to difficulty in the availability of large single crystals of Si_3N_4 and SiC, controlled experiments to understand the effect of orientation of the bounding grains on the IGF thickness are still lacking. Motivated by the occasional observation of orientation dependence of IGF thickness between hexagonal BN inclusions and β-SiC grains in Si_3N_4–SiC composites Knowles and Turan [122] extended Clarke's force balance theory [60] by orientation dependent terms. On the other hand, the effect of the orientation of the bounding grains on wetting of GBs by glass (with no formation of IGF) has been studied in the Al_2O_3 system [123]. Our understanding of this aspect is incomplete at this point of time. The picture is rather bimodal as it stands today: dry boundaries for low-angle and special (near Sigma) boundaries or boundaries with a film of equilibrium thickness.

5.4.5. Orientation of the interface plane

Very little is known about the effect of the orientation of the interface plane on the formation/thickness of the IGF. Hutt et al. [124] studying faceted, near $\Sigma = 3$ boundaries in polycrystalline Fe doped $SrTiO_3$ using HREM observed that one of the facets is parallel to the $\{1\,1\,1\}$ plane of the crystal and the other facet is inclined. The inclined facet showed a diffuse contrast implying disorder in the structure.

6. Outstanding issues and open questions

- IGFs represent equilibrium at which temperature?
- What is the precise dependence of orientation of the bounding grains on the film thickness?

- What is the exact structure of the glass-crystal interface? How can we perform an even better characterization of the amorphous material in the IGF? (Three-dimensional atomic structure of the IGF would be the ideal goal.)
- How are IGFs in various systems different from each other and what features of the IGF are system independent and can be studied by a universal model? And, if there are system dependent features can there be sub-classifications based electronic structure, bonding characteristics, etc.?
- How to develop a unified theory which would describe the thickness of IGFs as a function of temperature, activity of the chemical species and crystallography and also account for the internal structure within the IGF?
- How to predict the formation of IGF in new systems?

7. Summary

The study of intergranular glassy films has come a long way to warrant a separate place for it in literature distinct from disordered interfaces and extended grain boundaries. This has been possible via pioneering advances in experimental and theoretical techniques coupled with some innovative and systematic experimentation. However, at this stage complete understanding of these films still eludes the scientific community and research in the coming years will prove to be very important.

Acknowledgments

The financial assistance from the European Commission under contract Nr. G5RD-CT-2001-00586 is also acknowledged. Anandh Subramaniam wishes to acknowledge the Alexander von Humboldt foundation for their research fellowship. The authors thank Somnath Bhattacharyya for proving the high-resolution micrograph shown in Fig. 2.

References

[1] H.-J. Kleebe, J. Ceram. Soc. Jpn. 105 (1997) 453–475.
[2] H.-J. Kleebe, J. Eur. Ceram. Soc. 10 (1992) 151–159.
[3] R. Brydson, S.-C. Chen, F.L. Riley, S.J. Milne, X. Pan, M. Rühle, J. Am. Ceram. Soc. 81 (1998) 369–379.
[4] X. Pan, H. Gu, S. Stemmer, M. Rühle, Mater. Sci. Forum 207–209 (1996) 421–424.
[5] W.G. Morris, J. Am. Ceram. Soc. 56 (1973) 360–364.
[6] D.R. Clarke, J. Appl. Phys. 49 (1978) 2407–2411.
[7] C. O'Meara, J. Sjöberg, G. Dunlop, J. Eur. Ceram. Soc. 7 (1991) 369.
[8] H.D. Ackler, Y.M. Chiang, J. Am. Ceram. Soc. 80 (1997) 1893–1896.
[9] S. Kanzaki, T. Kumazawa, J. Asaumi, O. Abe, H. Tabata, J. Ceram. Soc. Jpn. 93 (1985) 407.
[10] Y.M. Chiang, L.A. Silverman, R.H. French, R.M. Cannon, J. Am. Ceram. Soc. 77 (1994) 1143–1152.
[11] K. Daschowdhury, R.W. Carpenter, W. Braue, Ultramicroscopy 40 (1992) 229–239.
[12] A. Avishai, C. Scheu, W.D. Kaplan, Z. Metallkd. 94 (2003) 272–276.
[13] H.G. Jeong, K. Hiraga, M. Mabuchi, K. Higashi, Philos. Mag. Lett. 74 (1996) 73–80.
[14] H.-J. Kleebe, M.J. Hoffmann, M. Rühle, Z. Metallkd. 83 (1992) 610–617.
[15] D.R. Clarke, G. Thomas, J. Am. Ceram. Soc. 60 (1977) 491–495.
[16] H. Schmid, M. Rühle, J. Mater. Sci. 19 (1984) 615–628.
[17] D.R. Clarke, J. Phys. 46 (C4) (1985) 51–58.
[18] J. Luo, Y.M. Chiang, J. Eur. Ceram. Soc. 19 (1999) 697–701.
[19] C.M. Wang, X. Pan, M.J. Hoffmann, R.M. Cannon, M. Rühle, J. Am. Ceram. Soc. 79 (1996) 788–792.
[20] H. Gu, R.M. Cannon, M. Rühle, J. Mater. Res. 13 (1998) 376–387.
[21] D.B. Williams, C.B. Carter, Transmission Electron Microscopy, Plenum Press, New York, 1996.
[22] D.R. Clarke, Ultramicroscopy 4 (1979) 33–44.
[23] S. Hofmann, L.J. Gauckler, Powder Metall. Int. 6 (1974) 90–92.
[24] B.D. Powell, P. Drew, J. Mater. Sci. 9 (1974) 1867–1870.
[25] S.H. Kim, H.T. Kim, J.H. Park, Y. Kim, Mater. Res. Bull. 34 (1999) 415–423.
[26] J.-H. Lee, T. Mori, J.-G. Li, T. Ikegami, S. Takenouchi, J. Eur. Ceram. Soc. 21 (2001) 13–17.
[27] G. Pezzotti, J. Non-Cryst. Solids 321 (2003) 37–51.
[28] G. Roebben, C. Sarbu, T. Lube, O. Van der Biest, Mater. Sci. Eng. A 370 (2004) 453–458.
[29] D.E. Newbury, D.B. Williams, Acta Mater. 48 (2000) 323–346.
[30] M.K. Cinibulk, H.-J. Kleebe, M. Rühle, J. Am. Ceram. Soc. 76 (1993) 426–432.
[31] I. MacLaren, Ultramicroscopy 99 (2004) 103–113.
[32] M. Döblinger, D.J.H. Cockayne, R.R. Meyer, A.I. Kirkland, D.N. Manh, in: D. Schryvers, J.-P. Timmermans (Eds.), Proceedings of the 13th European Microscopy Congress, vol. II, Belgian Society for Microscopy, Liège, 2004, pp. 59–60.
[33] A. Ziegler, C. Kisielowski, M.J. Hoffmann, R.O. Ritchie, J. Am. Ceram. Soc. 68 (2003) 1777–1785.
[34] D.B. Williams, A.D. Romig, Ultramicroscopy 30 (1989) 38–51.
[35] T. Walther, Ultramicroscopy 96 (2003) 401–411.
[36] H. Gu, X. Pan, R.M. Cannon, M. Rühle, J. Am. Ceram. Soc. 81 (1998) 3125–3135.
[37] K. Daschowdhury, R.W. Carpenter, W. Braue, J. Liu, H. Ma, J. Am. Ceram. Soc. 78 (1995) 2579–2592.
[38] H. Gu, Miran, S. Stemmer, H. Müllejans, M. Rühle, Ultramicroscopy 59 (1995) 215–227.
[39] N. Shibata, S.J. Pennycook, T.R. Gosnell, G.S. Painter, W.A. Shelton, P.F. Becher, Nature 428 (2004) 730–733.
[40] A. Ziegler, J.C. Idrobo, M.K. Cinibulk, C. Kisielowski, N.D. Browning, R.O. Ritchie, Science 306 (2004) 1768–1770.
[41] M. Elfwing, E. Olssona, J. Appl. Phys. 92 (2002) 5272–5280.
[42] D.R. Rasmussen, C.B. Carter, Ultramicroscopy 32 (1990) 337–348.
[43] Q. Jin, S. Wilkinson, G.C. Weatherly, J. Eur. Ceram. Soc. 18 (1998) 2281–2286.
[44] R.E. Dunin-Borkowski, Ultramicroscopy 83 (2000) 193–216.
[45] R. Vincent, Ultramicroscopy 90 (2000) 135–151.
[46] C.T. Koch, S. Bhattacharyya, M. Rühle, Microsc. Microanal. (2005), in press.
[47] J.M. Vitek, M.D. Vaudin, M. Rühle, S.L. Sass, Scripta Metall. 23 (1989) 349–354.
[48] C.T. Koch, S. Bhattacharyya, A. Subramaniam, M. Rühle, Microsc. Microanal. 10 (Suppl.) (2004) 254–255.
[49] C.T. Koch, Z. Metallkd. 96 (2005) 443–447.
[50] W. McBride, D.J.H. Cockayne, D. Nguyen-Manh, Ultramicroscopy 96 (2003) 191–200.
[51] M. Döblinger, C.D. Marsh, D. Nguyen-Manh, D. Ozkaya, D.J.H. Cockayne, Inst. Phys. Conf. Ser. 179 (2004) 401–404.
[52] C.T. Koch, S. Garofalini, Ultramicroscopy (2005), in press.
[53] S.J. Pennycook, M.F. Chisholm, A.R. Lupini, A.Y. Borisevich, M. Varela, Y. Peng, K.V. Benthem, Presentation in Session S3, MRS Spring Meeting, San Francisco, 2005.
[54] P.A. Midgley, M. Weyland, Ultramicroscopy 96 (2003) 413–431.
[55] M.P. Brada, D.R. Clarke, Acta Mater. 45 (1997) 2501–2508.
[56] M. Yoshiya, I. Tanaka, H. Adachi, Acta Mater. 48 (2000) 4641–4645.
[57] H.J. Choi, G.H. Kim, J.G. Lee, Y.W. Kim, J. Am. Ceram. Soc. 83 (2000) 2821–2827.
[58] J. Golczewski, F. Aldinger, A. Chang, M.T. Clavaguera-Mora, A. Rempel, E. Rudnyi, Z. Metallkd. 92 (2001) 560–562.
[59] J. Golczewski, H.J. Seifert, F. Aldinger, Z. Metallkd. 92 (2001) 695–700.

[60] D.R. Clarke, J. Am. Ceram. Soc. 70 (1987) 15–22.
[61] D.R. Clarke, T.M. Shaw, A. Philipse, R.G. Horn, J. Am. Ceram. Soc. 76 (1994) 1201–1204.
[62] J. Israelachvili, Intermolecular and Surface Forces, Academic Press, San Diego, 1992.
[63] D.F. Evans, H. Wennerström, The Colloidal Domain: Where Physics, Chemistry, Biology and Technology Meet, VCH Publishers Inc., New York, 1994.
[64] H.D. Ackler, Thermodynamic calculations and model experiments on thin intergranular amorphous films in ceramics, Ph.D. Thesis, Massachusetts Institute of Technology, Boston, 1997.
[65] H.D. Ackler, Y.M. Chiang, in: A.P. Tomsia, A. Glaeser (Eds.), Thin Intergranular Films in Ceramics: Thermodynamic Calculations and Model Experiments in the System Titania–Silica, Ceramic Microstructure: Control at the Atomic Level, Plenum Press, New York, 1998, pp. 149–160.
[66] J.W. Cahn, J.E. Hilliard, J. Chem. Phys. 28 (1958) 258–267.
[67] M. Bobeth, D.R. Clarke, W. Pompe, J. Am. Ceram. Soc. 82 (1999) 1537–1546.
[68] I. Tanaka, J. Ceram. Soc. Jpn. 109 (2001) S127–S134.
[69] R.M. Cannon, L. Esposito, Z. Metallkd. 90 (1999) 1002–1015.
[70] R.M. Cannon, Structure–Composition–Stability Relations in Ceramic Interfaces, Max Planck Institute, Stuttgart, 2004.
[71] R.M. Cannon, M. Rühle, M.J. Hoffmann, R.H. French, H. Gu, A.P. Tomsia, E. Saiz, Mater. Sci. Eng. A, this issue.
[72] C.M. Bishop, Continuum models for intergranular films in silicon nitride and comparison to atomistic simulations, Ph.D. Thesis, Massachusetts Institute of Technology, Boston, 2003.
[73] C.M. Bishop, W.C. Carter, Comput. Mater. Sci. 25 (2002) 378–386.
[74] R. Kobayashi, J.A. Warren, W.C. Carter, Physica D 119 (1998) 415–423.
[75] A. Sutton, personal communication, 2004.
[76] P. Keblinski, S.R. Phillpot, D. Wolf, H. Gleiter, J. Am. Ceram. Soc. 80 (1997) 717–732.
[77] S. Blonski, S.H. Garofalini, J. Am. Ceram. Soc. 80 (1997) 1997–2004.
[78] S. Garofalini, W. Luo, J. Am. Ceram. Soc. 86 (2003) 1741–1752.
[79] X. Su, S.H. Garofalini, J. Mater. Res. 19 (2004) 752–758.
[80] A.Z. Panagiotopoulos, J. Phys.: Condens. Matter 12 (2000) R25–R52.
[81] W. Kohn, L.J. Sham, Phys. Rev. A 140 (1965) 1133–1138.
[82] W.Y. Ching, J. Am. Ceram. Soc. 87 (2004) 1996–2013.
[83] P. Rulis, J. Chen, L. Ouyang, W.Y. Ching, X. Su, S.H. Garofalini, Phys. Rev. B, in press.
[84] W.Y. Ching, P. Rulis, L. Ouyang, Phys. Rev. B, submitted for publication.
[85] I. Tanaka, H.-J. Kleebe, M.K. Cinibulk, J. Bruley, D.R. Clarke, M. Rühle, J. Am. Ceram. Soc. 77 (1994) 911–914.
[86] H. Wang, Y.M. Chiang, J. Am. Ceram. Soc. 81 (1998) 89–96.
[87] Z. Zhang, unpublished result.
[88] H. Kessler, H.-J. Kleebe, R.W. Cannon, W. Pompe, Acta Metall. Mater. 40 (1992) 2233–2245.
[89] R. Raj, J. Am. Ceram. Soc. 64 (1981) 245–248.
[90] J. Luo, Y.M. Chiang, Acta Mater. 48 (2000) 4501–4515.
[91] Y.M. Chiang, Midterm report of nanometer scale induced structure between amorphous layers and crystalline materials (NANOAM), Project funded by the European Community, GRD2-CT-2000-30351, 2003.
[92] J. Luo, Y.M. Chiang, R.M. Cannon, Langmuir, in press.
[93] B.B. Straumal, P. Zięba, W. Gust, Int. J. Inorg. Mater. 3 (2001) 1113–1115.
[94] B. Straumal, B. Baretzky, Interface Sci. 12 (2004) 147–155.
[95] B.B. Straumal, S.I. Prokofjev, L.-S. Chang, N.E. Sluchanko, B. Barezky, W. Gust, E.J. Mittemeijer, Defect Diffus. Forum 194–199 (2001) 1343–1348.
[96] L.-S. Chang, E. Rabkin, B.B. Straumal, B. Barezky, W. Gust, Acta Mater. 15 (1999) 4041–4046.
[97] P.L. Flaitz, J.A. Pask, J. Am. Ceram. Soc. 70 (1987) 449–455.
[98] T.M. Shaw, P.R. Duncombe, J. Am. Ceram. Soc. 74 (1991) 2495–2505.
[99] J.R. Lee, Y.M. Chiang, Solid State Ionics 75 (1995) 79–88.
[100] Y.M. Chiang, J.-R. Lee, H. Wang, in: A.P. Tomsia, A. Glaeser (Eds.), Microstructure and Intergranular Phase Distribution in Bi_2O_3-Doped ZnO, Ceramic Microstructure: Control at the Atomic Level, Plenum Press, New York, 1998, pp. 131–147.
[101] G. Quinn, personal communication.
[102] Q. Jin, D.S. Wilkinson, G.C. Weatherly, W.E. Luecke, S.M. Wiederhorn, J. Am. Ceram. Soc. 84 (2001) 1296–1300.
[103] D.R. Clarke, J. Am. Ceram. Soc. 72 (1989) 1604–1609.
[104] M.K. Cinibulk, H.-J. Kleebe, G.A. Schneider, M. Rühle, J. Am. Ceram. Soc. 76 (1993) 2801–2808.
[105] M.K. Cinibulk, H.-J. Kleebe, in: A.P. Tomsia, A. Glaeser (Eds.), Grain-Boundary Films in Silicon Nitride Ceramic at High Temperatures, Ceramic Microstructure: Control at the Atomic Level, Plenum Press, New York, 1998, pp. 123–130.
[106] Z. Zhang, C.T. Koch, M. Rühle, Nanometer Scale Induced Structure between Amorphous Layers and Crystalline Materials (Meeting), Paris, 2004.
[107] S. Bhattacharyya, A. Subramaniam, C.T. Koch, M. Rühle, Mater. Sci. Eng. A, in press.
[108] M.K. Cinibulk, H.-J. Kleebe, J. Mater. Sci. 28 (1993) 5775–5782.
[109] D.R. Clarke, N.J. Zaluzec, R.W. Carpenter, J. Am. Ceram. Soc. 64 (1981) 608–611.
[110] A. Tsuge, K. Nishida, M. Komatsu, J. Am. Ceram. Soc. 58 (1975) 323–326.
[111] J.S. Vetrano, H.-J. Kleebe, E. Hampp, M.J. Hoffmann, M. Rühle, R.M. Cannon, J. Mater. Sci. 28 (1993) 3529–3538.
[112] X.F. Zhang, M.E. Sixta, L.C. De Jonghe, J. Am. Ceram. Soc. 83 (2000) 2813–2820.
[113] C.M. Wang, M. Mitomo, T. Nishimura, Y. Bando, J. Am. Ceram. Soc. 80 (1997) 1213–1221.
[114] R.L. Satet, M.J. Hoffmann, Key Eng. Mater. 264–268 (2004) 775–780.
[115] G.D. Quinn, J. Mater. Sci. 25 (1990) 4361–4376.
[116] T. Gemming, S. Nufer, W. Kurtz, M. Rühle, J. Am. Ceram. Soc. 86 (2003) 581–589.
[117] A. Alessandrini, G. Valdre, B. Morten, M. Prudenziati, J. Appl. Phys. 92 (2002) 4705–4711.
[118] M. Hrovat, Z. Samardzija, J. Holc, D. Belavic, J. Mater. Sci. 37 (2002) 2331–2339.
[119] E. Olsson, G.L. Dunlop, J. Appl. Phys. 66 (1989) 3666–3675.
[120] X. Pan, J. Meyer, M. Rühle, K. Niihara, J. Am. Ceram. Soc. 79 (1996) 585–590.
[121] H.-J. Kleebe, M.K. Cinibulk, R.M. Cannon, M. Rühle, J. Am. Ceram. Soc. 76 (1993) 1969–1977.
[122] K.M. Knowles, S. Turan, Ultramicroscopy 83 (2000) 245–259.
[123] B.J. Hockey, S.M. Wiederhorn, J.E. Blendell, J.S. Lee, M.K. Kang, J. Am. Ceram. Soc. 86 (2003) 612–622.
[124] S. Hutt, O. Kiensle, F. Ernst, M. Rühle, Z. Metallkd. 92 (2001) 105–109.